Characterizing Volcanic Ash Density and its Implications on Settling Dynamics

Sing Lau[1], Roy G. Grainger[2], Isabelle A. Taylor[2]

[1]Atmospheric, Oceanic, & Planetary Physics, University of Oxford, OX1 3PU, Oxford, U.K.
[2]COMET, Atmospheric, Oceanic and Planetary Physics, University of Oxford, Oxford, OX1 3PU, U.K.

Key Points:

- The density of volcanic ash is measured as a function of particle size for a range of eruptions.
- Silica content and particle size negatively correlate with density.
- The density of particles smaller than 100 µm is approximately constant but is dependent on silica content.

Corresponding author: Sing Lau, `woonsinglau@gmail.com`

Abstract

Volcanic ash clouds are carefully monitored as they present a significant hazard to humans and aircraft. The primary tool for forecasting the transport of ash from a volcano is dispersion modelling. These models make a number of assumptions about the size, sphericity and density of the ash particles. Few studies have measured the density of ash particles or explored the impact that the assumption of ash density might have on the settling dynamics of ash particles. In this paper, the raw apparent density of 23 samples taken from 15 volcanoes are measured with gas pycnometry, and a negative linear relationship is found between the density and the silica content. For the basaltic ash samples, densities were measured for different particle sizes, showing that the density is approximately constant for particles smaller than 100 µm, beyond which it decreases with size. While this supports the current dispersion model used by the London Volcanic Ash Advisory Centre (VAAC), where the density is held at a constant (2.3 g cm^{-3}), inputting the measured densities into a numerical simulation of settling velocity reveals a primary effect from the silica content changing this constant. The VAAC density overestimates ash removal times by up to 18 %. These density variations, including those varying with size beyond 100 µm, also impact short-range particle-size distribution (PSD) measurements and satellite retrievals of ash.

Plain Language Summary

Volcanic ash clouds are carefully monitored as they present a significant hazard to humans and aircraft. Dispersion modelling is a primary tool used to forecast ash flows from volcanoes. These models make a number of assumptions about the size, sphericity (roundness) and density of the ash particles. Few studies have measured the density of ash particles or explored the impact that the assumption of ash density might have on the dispersion forecasts. In this paper, the density of 23 samples taken from 15 volcanoes are measured, and a negative linear relationship is found between the density and the silica content. For the basaltic ash samples (the most common type of ash), densities were measured for different particle sizes, showing that the density is approximately constant for particles smaller than 100 µm, beyond which it decreases with size. This supports the London Volcanic Ash Advisory Centre (VAAC) keeping density constant in their current model, but in fact this constant changes with silica content, leading to an overestimation of ash removal times by up to 18 %. These density deviations also impact short-range particle-size distribution (PSD) measurements and satellite retrievals of ash.

1 INTRODUCTION

Volcanic ash is composed of hard, silicic and abrasive fragments of rock, minerals, and glass. During explosive volcanic eruptions, dissolved gases in magma are heated and expand abruptly, shattering a large amount of magma and rock materials into pyroclast fragments (Kenedi, 2000). These pyroclasts can be catagorized according to diameter into fine ash ($< 30-60$ µm), ash (< 2 mm), lapilli (2-64 mm), bombs (> 64 mm) (Rose & Durant, 2009; Fisher & Schmincke, 1984). The size of these particles often have the same order of magnitude as the gas bubble that shattered them, and since there is a lower limit of the size of gas bubbles, ash smaller than a few microns are rarely found (Sparks & Wilson, 1976; Rust & Cashman, 2011).

Volcanic ash is harmful to humans when inhaled (Gislason et al., 2011; Horwell & Baxter, 2006; Horwell, 2007), and it poses a risk to aviation even at a large distance from the vent (Casadevall, 1994; Dunn & Wade, 1994; Pieri et al., 2002; Guffanti & Tupper, 2015). For example, during the 2010 Eyjafjallajökull eruption, a large area of airspace over Europe was closed for several days to minimize the risk to aviation, causing significant financial losses (Rincon, 2011). This eruption provided the impetus for further de-

velopment of existing dispersion models, measurements, and approaches to manage these hazards. (Beckett et al., 2020).

The London Volcanic Ash Advisory Centre (VAAC) provides analysis of volcanic ash dispersion in the North Atlantic and Arctic area, including countries such as the United Kingdom and Iceland. Together with other VAACs around the world, it use a range of measurements, satellite observations, and models to study eruptions, with the primary objective of mitigating aviation risk from ash clouds (Beckett et al., 2020).

The size, shape and density of ash particles have all been shown to influence the maximum travel distance of volcanic ash (Beckett et al., 2015). However, density is usually assigned an assumed value due to limited measurements. The London VAAC uses a constant density of 2.3 g cm^{-3} in their operational dispersion model, Numerical Atmospheric-dispersion Modelling Environment (NAME), which focuses on ash smaller than 100 µm in diameter (Beckett et al., 2020). The ash density is also assumed when estimating the total mass of ash from satellite data (Beckett et al., 2017). In addition, when exploiting the Doppler shift of ash particles for determining the fall velocity and hence particle-size distribution (PSD), the results are very sensitive to the assumptions on density (Bonadonna et al., 2011).

There are multiple definitions of density (Webb & Orr, 1997; Vogel et al., 2017). The following definitions are adopted here:

- Bulk density takes the total volume enveloping the entire particle sample, including voids between particles.
- Apparent / skeletal density takes the volume of the particle including closed pores (pores that are sealed off from the outside) but excluding open pores.
- Dense-rock-equivalent (DRE) / true density takes the volume of the particle excluding both open and closed pores. It measures the net density of the solid fraction.

While travelling in the atmosphere, air molecules may seep into the open pores but not the closed pores of ash particles. Therefore the aerodynamically meaningful density comes from the skeletal structure. Unless otherwise stated, this work uses density to mean the apparent density.

Variations in density may orginate from i) composition, and ii) porosity inside the particle. Ash particles generally follow the composition of the magma they originate from. They can be classified by a total alkali-silica (TAS) diagram, which plots K_2O/ Na_2O (alkaline) versus SiO_2 (silica) content for volcanic rocks. Alkalinity in volcanic ash is relatively low in the TAS diagram, such that it is sufficient to group ash into four major types of magma based on silica content (Krishnan et al., 2017). In terms of percentage SiO_2 by weight, they are basalts (41-54 %), andesites (54-63 %), dacites (63-70 %), and rhyolites (65-75 %) (M. Wilson, 1989). The boundaries are not clear-cut: for example "basalt-andesites" would describe a transitional composition between the two categories. Vogel et al. (2017) used water pycnometry to show that the DRE density decreases with a linear trend as silica content increases, suggesting that silica content can be the dominant predictor of density of non-porous pyroclasts.

While silica-rich magma has higher dissolved gas content, it is also more viscous, enabling more explosive eruptions (Parfitt & Wilson, 2009). This process further introduces gas into the solidifying pyroclast, causing the pumice and ash formed from these magma to be more porous. Porosity and particle size are also closely related. If a large porous pyroclast breaks down into smaller pieces, the larger fragments could encapsulate more and larger closed pores and hence have a lower density. Therefore, a decreasing density is expected with increasing size for a given ash composition.

Finer particles can travel a long distance in air before falling out, and fuse with larger grains that act as a core in a process known as aggregation (Rossi et al., 2021). This effect altering the particle size and density, but it is prominent only when the particle concentration is high (Del Bello et al., 2017), so any identified aggregates are measured separately.

Many prior studies used simplified density-size models: for example, L. Wilson and Huang (1979) studied clasts collected from the equatorial Pacific and São Miguel, Portugal; measuring the dimensions of particles individually. They presented a model which fixed the densities for large (>300 µm) and small (<88 µm) particles, and fitted densities for intermediate sizes with linear interpolation (shown in Figure 1 as 'General model').

In the basaltic range, Beckett et al. (2015) established a density model based on scattered data from Eyjafjallajökull in Bonadonna et al. (2011). It used a piece-wise linear fit to interpolate the sparse data, and is referred to as 'EYJ 2010 model' in Figure 1 and the rest of this paper.
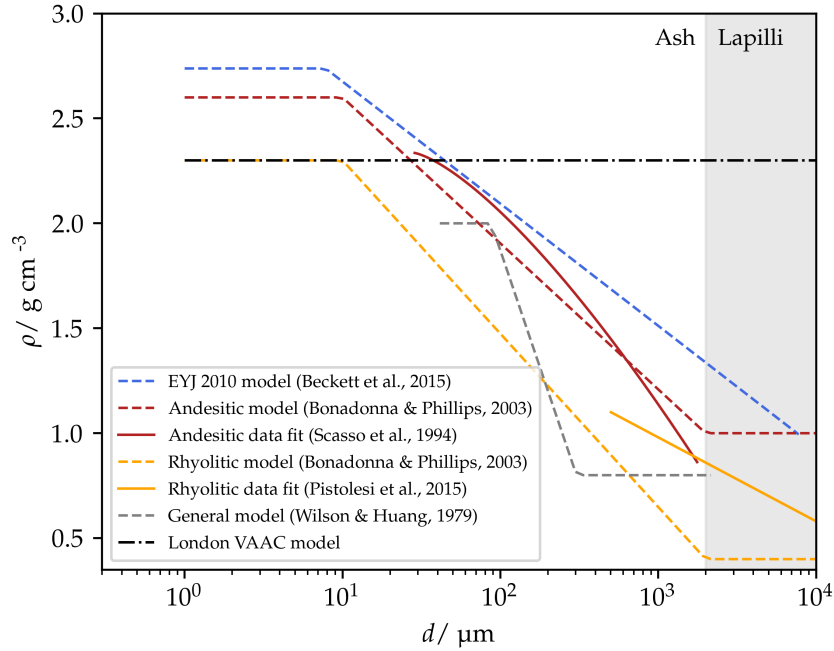

Figure 1. Summary of representative current models and data relating apparent density ρ and particle diameter d.

In the andesitic range, Bonadonna and Phillips (2003) presented another model ('andesitic model' in Figure 1), similarly interpolated, based on scattered data from the 1991 eruption of Mount Hudson in Scasso et al. (1994). The original scattered data measured how the mean particle diameter and the apparent density of unsieved ash samples varied with distance from the vent. The samples consisted of a mix of all ash sizes, and the data points for the two measured quantities were attributed to different distances; therefore, only a rough trend line can be inferred by relating the lines of best fit, and is presented in Figure 1 as 'andesitic data fit'.

In the rhyolitic range, Bonadonna and Phillips (2003) interpolated a similar model based on scattered data from Askja, provided in Sparks et al. (1997); this model is presented in Figure 1 as 'rhyolitic model'. Pistolesi et al. (2015) measured density using wa-

ter pycnometry of ash from the 2011 Cordón Caulle eruption, Chile. They showed an approximately linear decrease between log diameter and density for pyroclast diameters between 500 and 16,000 µm ('rhyolitic data fit' in Figure 1), providing some support for linear models. However, water pycnometry does not measure apparent density well (Richards & Bouazza, 2007), and the minimum particle size measured was 500 µm, which is larger than a lot of ash produced.

Measurements of larger pyroclasts have been more abundant than ash. For example, Sparks et al. (1981) measured larger pyroclasts from the 1875 Askja eruption, and found that density generally decreases with size for diameters between 11,000 to 90,000 µm. Despite these findings, the detailed relationship between particle size and density has remained incomplete. In many cases, the diameter coverage was partial; some relied on other assumed relationships or water pycnometry.

In this study, the density of 22 ash samples from 15 volcanoes measured with a pycnometer, are presented. The measured densities are compared with the ash composition, and for some of the samples, against the particle size. Finally, the implications of density variations on ash settling dynamics, and the impacts of applying these measured density in dispersion models are explored.

2 METHODOLOGY

2.1 Ash Density Measurements

Apparent density measurements were conducted using a nitrogen gas pycnometer. Gas pycnometry applies the ideal gas law to determine the skeletal volume of samples in a chamber by varying the size of the chamber and measuring the pressure change (Webb & Orr, 1997). Nitrogen is used to best study the apparent density and permeability of the ash particles in the atmosphere (open pores that are smaller than its molecular size will be discounted). Water vapour affects both the actual density and the ideal gas law calculations, so the ash samples were dried in a 98°C oven for over 48 hours to ensure moisture was sufficiently evaporated. While humidity varies in the atmosphere, this study aims to provide a standardized perspective by measuring the dry density.

Two sets of measurements were conducted:

1. The density of 23 unsieved raw ash samples originating from 15 volcanoes around the world were measured. Table 1 and Figure 2 present their locations and specify the abbreviations used for the samples. To ensure fair representation, the original jars of raw ash were gently mixed by rotation. When extracting samples to measure in the pycnometer, large (~ 8 mm) outliers were not included. The details of the samples are recorded in Reed (2016) alongside silica content.
2. Volcanic ash is most commonly basaltic (Walker, 1993), and our basaltic samples are large enough to be further sieved for measurements. In particular, samples from Mount Aso (VA1), Eyjafjallajökull (VA7), and Grímsvötn (VA4, 5) were sieved into different diameter groups. For larger particles (> 2 mm in diameter), particles were handpicked and measured with a caliper. Densities were then measured for each particle size sample. For Grímsvötn, two sets of samples, from close (200 m from vent) to distal region (50 km from vent) are measured. There is a one-week interval between the collection dates of these two samples.

2.2 Fall Velocity and Time of flight

The measured data are used to compute fall velocity and time of flight in the atmosphere, with atmospheric data at different altitudes interpolated from the US Standard Atmosphere (NASA, 1976).
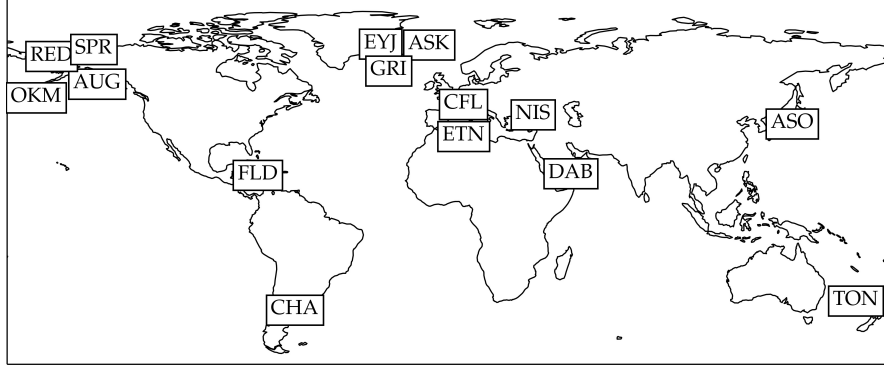
Figure 2. A map showing the 15 sources of 23 ash samples. Abbreviations and information are detailed in Table 1.

The general expression for drag force F_D on a particle with cross-sectional area A, travelling at velocity v in a fluid with density ρ_f and dynamic viscosity η is:

$$F_\mathrm{D} = \frac{1}{2} C_\mathrm{D} \rho_\mathrm{f} A v^2 \tag{1}$$

where C_D represents the drag coefficient. The particle reaches terminal velocity when its own weight balances out with this drag force and buoyancy. Assuming a spherical particle with diameter d, apparent density ρ and gravitational acceleration g:

$$\frac{4}{3}\pi \left(\frac{d}{2}\right)^3 (\rho - \rho_\mathrm{f})g = \frac{1}{2} C_\mathrm{D} \rho_\mathrm{f} A v^2 \tag{2}$$

implying that the terminal velocity v_T is

$$v_T = \sqrt{\frac{4}{3 C_\mathrm{D}} \frac{\rho - \rho_\mathrm{f}}{\rho_\mathrm{f}} dg} \tag{3}$$

C_D itself depends on the Reynold's number Re, defined as

$$Re = \frac{v d \rho_\mathrm{f}}{\eta} \tag{4}$$

White and Majdalani (2006) describes the drag coefficient for spherical particles for Re between 0 and 2×10^5 with

$$C_\mathrm{D} = \frac{24}{Re} + \frac{6}{1 + \sqrt{Re}} + 0.25 \tag{5}$$

In general, ash particles are sufficiently small such that terminal velocity can be treated as a constant fall velocity (also known as settling velocity). Therefore, this set of equations explicitly determines the settling velocity of spherical particles (and hence the time of flight and maximum drift distance). A non-spherical particle falls at a lower speed than its spherical equivalent, increasing the dispersion range (Beckett et al., 2015). For example, a 30 μm particle with sphericity $\Psi = 0.4$ travels $30\,\%$ further than its spherical counterpart.

Table 1. **Raw unsieved ash density** All ρ_{us} have a 2 % uncertainty. The list of respective magma and ash type is gathered from Miyabuchi et al. (2006); Keiding and Sigmarsson (2012); Haddadi et al. (2017); Andronico et al. (2009); Lara (2009); Field et al. (2008); Cole et al. (2018); Sparks et al. (1981); Wehrmann et al. (2006); Longchamp et al. (2011); Francalanci et al. (1995); Larsen et al. (2013, 2010); Eichelberger et al. (1995); Nye et al. (1994); Esposito et al. (2018). Uncertainties in SiO₂ are taken as 1%, the typical maximum uncertainty of XRF analysis (Rousseau, 2001).

Volcano (Abbrev.)	No.	Type	Distance from vent	Collection date	Estimated eruption	% SiO$_2$	ρ_{us}/ g cm^{-3}
Mount Aso, Japan (ASO)	VA1	Basaltic	< 400 m	1993	1993	52.6	2.80
Eyjafjallajökull, Iceland (EYJ)	VA2	Basaltic	6 km	17/4/2010	2010	55.6	2.65
Eyjafjallajökull, Iceland (EYJ)	VA3	Basaltic	-	4/2010	14/4/2010	57.8	2.68
Eyjafjallajökull, Iceland (EYJ)	VA7	Basaltic	5 km	13/6/2010	19-20/5/2010	58.5	2.57
Eyjafjallajökull, Iceland (EYJ)	VA8	Basaltic	4.5 km	13/6/2010	19-20/5/2010	59.2	2.66
Eyjafjallajökull, Iceland (EYJ)	VA9	Basaltic	5 km	13/6/2010	19-20/5/2010	58.8	2.62
Eyjafjallajökull, Iceland (EYJ)	VA15	Basaltic	-	15-16/5/2010	2010	58.0	2.68
Grímsvötn, Iceland (GRI)	VA4	Basaltic	200 m	1/6/2011	21-28/5/2011	49.1	2.76
Grímsvötn, Iceland (GRI)	VA5	Basaltic	50 km	25/5/2011	21-28/5/2011	49.4	2.76
Mount Etna, Italy (ETN)	VA6	Basaltic	10 km	27-30/12/2002	10/2022-1/2023	47.0	2.58
Mount Etna, Italy (ETN)	VA10	Basaltic	-	1/7/2001	10/2022-1/2023	47.6	2.83
Mount Etna, Italy (ETN)	VA14	Basaltic	26 km	1/11/2002	10/2022-1/2023	47.1	2.85
Chaitén, Chile (CHA)	VA11	Rhyolitic	-	2008	2008	73.2	2.36
Dabbahu, Ethiopia (DAB)	VA12	Rhyolitic	Very close	9/2005	26/9/2005	71.1	2.37
Mount Tongariro, New Zealand (TON)	VA16	Andesitic	-	2012	2012	59.4	2.60
Askja, Iceland (ASK)	VA17	Rhyolitic	-	1981	1875	70.7	2.35
Fontana Tephra, Nicaragua (FLD)	VA18	Basalt-andesitic	-	-	Late Pleistocene	-	2.62
Nisyros, Greece (NIS)	VA19	Rhyo-dacitic	-	2011	-	69.7	2.42
Mount Okmok, Alaska, USA (OKM)	VA20	Basalt-andesitic	-	7/2008	7/2008	-	2.74
Augustine, Alaska, USA (AUG)	VA21	Andesitic	-	13/1/2006	2005-2006	-	2.64
Mount Spurr, Alaska, USA (SPU)	VA22	Basalt-andesitic	-	8/1992	6-8/1992	-	2.73
Mount Redoubt, Alaska, USA (RED)	VA23	Andesite-dacitic	-	1990	1989-1990	-	2.68
Campi Flegrei, Italy (CFL)	VA24	Basaltic	-	-	-	-	2.42

204 **3 RESULTS**

205 **3.1 Unsieved ash density**

206   Table 2 presents the skeletal densities of the 23 unsieved ash samples. The raw data
207 can be accessed from Lau et al. (2023) or Supporting Information: Dataset S1. Mass per-
208 centage of SiO_2 content values were measured using X-ray fluorescence (XRF) analysis
209 by G. Prata et al. (2019). Figure 3 shows the measured unseived ash density ρ_{us} versus
210 silica content (%SiO_2). Before fitting a straight line, an outlier from Mount Etna con-
211 taining a large amount of biomass was removed. The results show that higher silica con-
212 tent correlates to a lower density in a linear relationship,

213
$$\rho_{us} = -0.016(\%SiO_2) + 3.54. \tag{6}$$

214 The function between DRE density ρ_{DRE} and silica content measured by Vogel et al. (2017)
215 is

216
$$\rho_{DRE} = -0.019(\%SiO_2) + 3.90. \tag{7}$$

217 Given the similarity of these correlations and ρ_{us} having a lower offset than ρ_{DRE} sug-
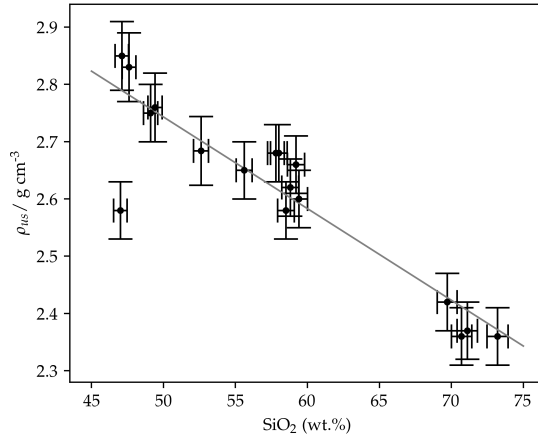218 gest porosity plays a systematic role in determining ash density.

Figure 3.   Unseived ash density versus silica content. A line of best-fit can be described by
ρ_{us} = $-0.016(\%SiO_2)$ + 3.54. An obvious outlier (lower left) has been removed from the fit.
It is a sample from Mount Etna which contains a large amount of biomass that is hard to re-
move. Uncertainties in SiO_2 are taken as 1 %, the typical maximum uncertainty of XRF analysis
(Rousseau, 2001). Uncertainty in ρ_{us} is 2 %.

219 **3.2 Density-size distribution**

220   Figure 4 shows the measured relationships between particle size and density for Ey-
221 jafjallajökull, Grímsvötn, and Mount Aso ash samples. The raw data can also be accessed
222 from Lau et al. (2023) or Supporting Information: Dataset S1. The densities follow a
223 similar pattern being constant at lower particle sizes, and then decreasing as the size in-
224 creases. To fit the data, two candidate models were tried: piece-wise linear (PL), and
225 smooth piece-wise quadratic (SPQ). Samples with fewer than 10 particles were excluded
226 from the fits. Writing $x = \log d$ where d is in µm, these models are specified respectively
227 as:

$$\rho = \begin{cases} k & x < x_0 \\ m(x - x_0) + k & x \geq x_0 \end{cases} \tag{8}$$

$$\rho = \begin{cases} k & x < x_0 \\ m(x - x_0)^2 + k & x \geq x_0 \end{cases} \tag{9}$$
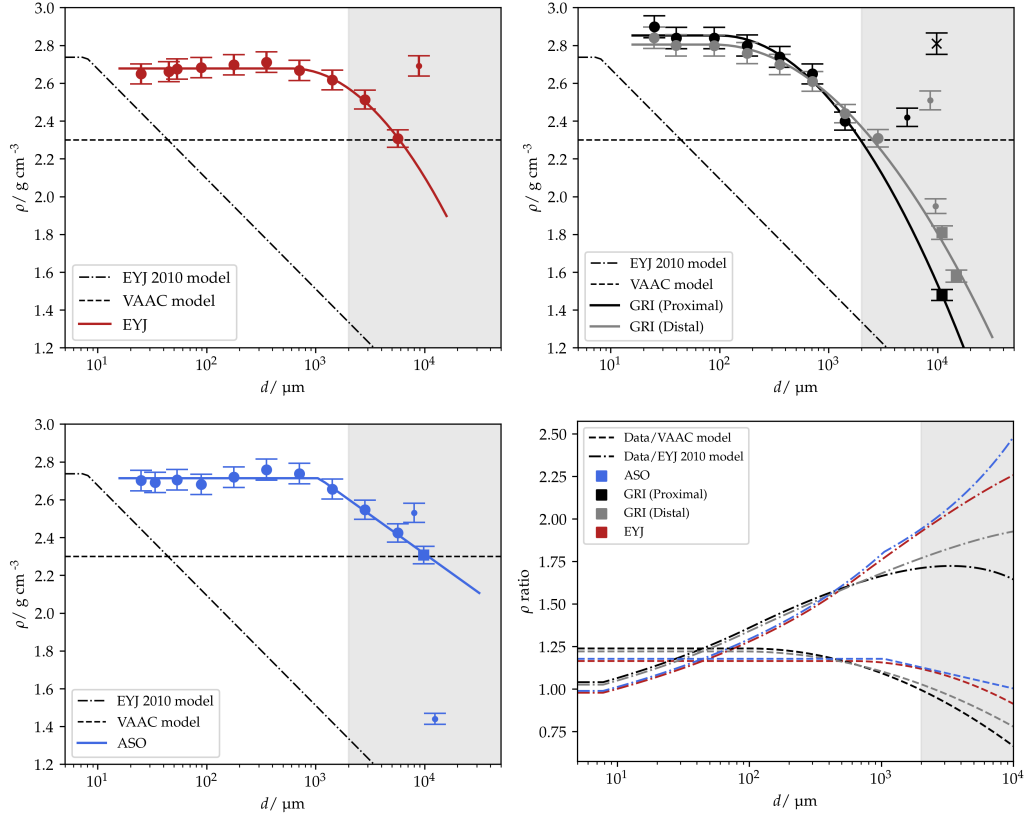

Figure 4. Particle density-size distribution for Eyjafjallajökull (EYJ), Grímsvötn (GRI Proximal/ Distal), and Mount Aso (ASO), alongside lines of best fit following either a piece-wise linear or a smooth piece-wise quadratic function (Equations 10-13). Models by London VAAC and one assumed by Bonadonna et al. (2011) ("EYJ 2010 model") are overlaid on the diagrams. Large circle markers indicate regular samples; squares and small circles indicate small (<10 particles) and single-particle samples. A cross in the second diagram indicates aggregates. Only the regular samples are used in fitting the functions. The fourth diagram shows the ratio of the four measured density fits versus the two referenced models. The shaded region in each graph concerns particles formally defined as "lapilli" instead of "ash".

Naturally one would expect a smooth transition between the flat and the sloping parts of the function, but owing to the preferable simplicity of the PL model, smoothness can be compromised. For the SPQ model, smoothness is demanded by setting the formula in this form. Both models have three parameter degrees of freedom (k, m, x_0). A reduced chi-squared test is performed to determine the better model for each source. The best model for each one is (in g cm⁻³):

Eyjafjallajökull (SPQ, $\chi^2 = 0.143$):

$$\rho = \begin{cases} 2.68 & x < 2.78 \\ -0.39(x - 2.78)^2 + 2.68 & x \geq 2.78 \end{cases} \tag{10}$$

Grímsvötn (Proximal—200 m from vent) (SPQ, $\chi^2 = 0.150$):

$$\rho = \begin{cases} 2.85 & x < 1.99 \\ -0.33(x - 1.99)^2 + 2.85 & x \geq 1.99 \end{cases} \tag{11}$$

Grímsvötn (Distal—50 km from vent) (SPQ, $\chi^2 = 0.848$):

$$\rho = \begin{cases} 2.81 & x < 1.94 \\ -0.24(x - 1.94)^2 + 2.81 & x \geq 1.94 \end{cases} \tag{12}$$

Aso (PL, $\chi^2 = 0.204$):

$$\rho = \begin{cases} 2.71 & x < 2.64 \\ -0.23(x - 2.64) + 2.71 & x \geq 2.64 \end{cases} \tag{13}$$

The constant portions confirm again that the higher the silica content, the lower the DRE density.

For Eyjafjallajökull, the samples were collected 6 km away from the vent. The measurements of finer ash plateaus to a similar DRE density as the EYJ 2010 model and other models presented in Figure 1. A striking difference is that the density starts decreasing at a much larger diameter (around 600 µm) than the EYJ 2010 model assumed (10 µm) (Figure 4, top left). In fact, measurements from all three sources support a later turning point than the previous models.

For Grímsvötn, the density plots are similar for ash samples collected at 200 m and 45 km from vent (Figure 4, top right), suggesting that the density is unlikely to be sensitive to sampling location (cf. grain size distribution). This would also suggest that one does not need to collect an excessive amount of samples to characterize ash density from an eruption.

For Aso, a PL model is adopted, contrary to the prior two sources (Figure 4, bottom left). However, the difference in function is most likely statistical, as the χ^2 evaluated with the two candidate functions are very close. The sample contains a mix of different colours, suggesting a wide range of compositions which may vary in abundance in difference size groups.

The measurements show that individual variations in density can be quite large. This is unsurprising as the existence of pores in a particle is probabilistic. Bonadonna and Phillips (2003) suggest that while pumice particle density would decrease substantially, lithic particles, which are a minor composition in ash, have a constant density. This is consistent with our data. Aggregates are also denser than individual particles on the same size, as they are composed of fine particles held together with much smaller closed pores.

Although silica-rich ash (e.g. Aso) are more porous, density falls off slower. Together with the observation from the silica content before, this suggests the dual role of pores—while more pores might lead to a hollower structure (lower density), to a certain extent the open pores might be populous enough to connect through the inner pores, discounting them from the particle volume and increasing density.

²⁷⁴ ## 4 IMPLICATIONS

²⁷⁵   To assess how the new density measurements will affect ash settling dynamics, Equa-
²⁷⁶ tions (1)-(5) were used to estimate settling velocity for spherical ash particles. Figure 5
²⁷⁷ shows settling velocity v_T as a function of particle diameter for the EYJ 2010 model, the
²⁷⁸ VAAC model, and the new density data. The values of ρ_f and η at zero altitude from
²⁷⁹ the US Standard Atmosphere (NASA, 1976) were used as an estimation. There is a max-
²⁸⁰ imum of 40 % difference between the v_T calculated from the measurements and the VAAC
²⁸¹ density in the ash range (<2000 µm); even only in the fine ash range ($\sim$10 µm), a max-
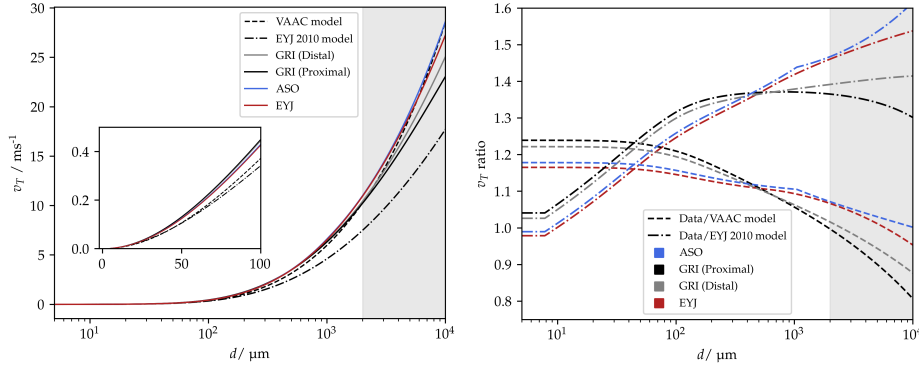²⁸² imum of 25% difference can be found.

Figure 5.   The left panel presents the settling velocity v_T versus particle diameter d calculated using the new density measurement fits (Equations 10-13) and the predictions of the VAAC and EYJ 2010 models. A zoom for d between 0 and 100 µm is included. The right panel shows the ratio between the calculated v_T and the model predictions (i.e. the solid coloured lines divided by the dashed lines in the left panel). The shaded region in each graph concerns particles formally defined as "lapilli" instead of "ash".

²⁸³   This substantially modifies the relationship between settling velocity and particle
²⁸⁴ size, which is crucial in dispersion models. Beckett et al. (2015) compared the EYJ 2010
²⁸⁵ model and the VAAC model at particle diameters of 30 and 100 µm using NAME. At
²⁸⁶ these sizes, densities from these two models differ by 4-9 %. This leads to a 4-8 % dif-
²⁸⁷ ference in v_T and a 4 % simulated difference in maximum horizontal distance D from the
²⁸⁸ vent reached by the particles for the Eyjafjallajökull eruption. For the same volcanic source,
²⁸⁹ the new density measurements show a 17 % difference from VAAC values for both these
²⁹⁰ sizes, implying a 14-16 % difference in v_T . This suggests a change in D above 10 % de-
²⁹¹ pending on the atmosphere; other processes that are considered in operational disper-
²⁹² sion models, such as atmospheric stability, wind, and aerosol microphysics, have not been
²⁹³ included in this estimation. The fact that VAAC currently uses the same density for all
²⁹⁴ events causes an even larger difference for some sources—for example, within the particle-
²⁹⁵ size range of NAME (<100 µm), the measured ash densities from Grímsvötn (Proximal)
²⁹⁶ would give a 20-23 % difference in v_T from the VAAC model. This arises from density
²⁹⁷ variations with silica content (Figure 3).

²⁹⁸   An alternative method to assess density effects is through calculating the time of
²⁹⁹ flight of particles. Grímsvötn (Proximal) ash density is used in this simulation as it de-
³⁰⁰ viated the most from the VAAC model (Figure 5). Neglecting aggregation, Figure 6 shows
³⁰¹ the time $t_{fallout}$ it takes for ash of different diameters to fall from an initial height of 20
³⁰² km. The right panel also shows the ratio of this fallout time predicted by the various dis-
³⁰³ tributions. Results show that the measured ash would fallout up to 18 % quicker than

in the VAAC model. For example, 10 μm fine ash would be removed from the plume five days earlier than the VAAC prediction, which is a significant modification for decision-making such as airspace closures.

Figure 6 also demonstrates that an unsieved density (corresponding to Table 1) used for all particle sizes approximates the behaviour of the exact density function well for particles smaller than 100 μm. This reiterates that while the size-density relationship might be a secondary factor to finer ash dispersion, density variations due to silica content could not be ignored. Although obtaining sample densities close to eruption times is a challenge, the results suggest that even a coarse density estimate based on, for example, underlying magma type, could improve the simulations reasonably.
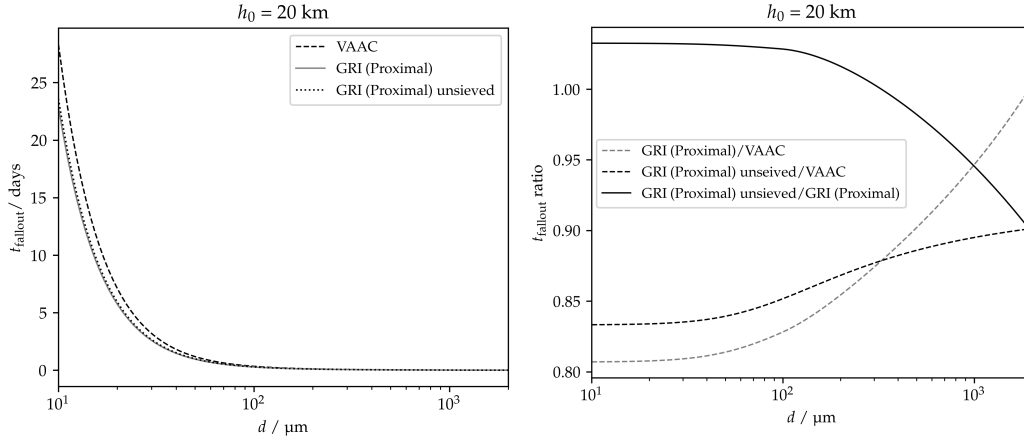

Figure 6. Fallout time from an altitude of 20 km of the characterized proximal ash from Grímsvötn (GRI), in comparison with the VAAC model. In addition, a model (GRI unsieved) where the unsieved ash density (Table 1) is kept constant is compared here. Atmospheric data at different altitudes are interpolated from the US Standard Atmosphere (NASA, 1976).

Moreover, a direct impact of the relationship between fall velocity and size is a change in the short-range measurement of particle-size distribution based on the Doppler effect (Bonadonna et al., 2011). The EYJ 2010 model is an example of a calibrating model that correlates density with size, and hence terminal velocity with size according to Equation (3). For larger particles from Grímsvötn (Proximal), a 40% difference in attributed fall velocity from the EYJ 2010 model could lead to a two-fold difference in the PSD (Figure 6). Satellite retrievals of ash using infrared measurements will also be impacted by improved estimates of density as the estimate of mass loading is a linear function of density. For example A. Prata et al. (2022) used a density of $2.3\,\mathrm{g\,cm^{-3}}$ to estimate mass loading for the 2019 Raikoke eruption. Measurements of airfall ash give a SiO_2 content of $\sim50\,\%$ (Smirnov et al., 2021) implying an ash density from Equation (6) of $2.74\,\mathrm{g\,cm^{-3}}$, i.e. a 18 % difference in the estimate of mass loading.

5 CONCLUSION

Density measurements of ash particles with nitrogen gas pycnometry have revealed a notable deviation from previous models. The measured density decreases for larger particles due to increased closed pores, while generally decreasing with larger silica content. However, this decrease due to size takes place prominently only for diameters substantially greater than 100 μm, before which the density remains constant at the DRE value.

While this supports the London VAAC using a constant density within the particle size range of NAME, silica content changes this constant. In the basaltic ash range studied, this behaviour leads to a settling velocity deviation of up to $23\,\%$ from the current VAAC density model for dispersion analysis, and up to around $40\,\%$ from the EYJ 2010 model, an example that can be used to infer PSD. The results demonstrate the importance of characterizing ash density in dispersion forecasts, satellite retrievals and other velocity-sensitive tasks.

6 Open Research

The raw data of density measurements in the study are available (open access) at Oxford University Research Archive (ORA) via DOI 10.5287/ora-r1dqbnpab (Lau et al., 2023), or in Supporting Information: Dataset S1.

References

Andronico, D., Cristaldi, A., Del Carlo, P., & Taddeucci, J. (2009). Shifting styles of basaltic explosive activity during the 2002–03 eruption of Mt. Etna, Italy. *Journal of Volcanology and Geothermal Research*, *180*(2-4), 110–122.

Beckett, F., Kylling, A., Sigurðardóttir, G., von Löwis, S., & Witham, C. (2017). Quantifying the mass loading of particles in an ash cloud remobilized from tephra deposits on iceland. *Atmospheric Chemistry and Physics*, *17*(7), 4401–4418.

Beckett, F., Witham, C., Hort, M., Stevenson, J., Bonadonna, C., & Millington, S. (2015). Sensitivity of dispersion model forecasts of volcanic ash clouds to the physical characteristics of the particles. *Journal of Geophysical Research: Atmospheres*, *120*(22), 11–636.

Beckett, F., Witham, C., Leadbetter, S., Crocker, R., Webster, H., Hort, M., . . . Thomson, D. (2020). Atmospheric dispersion modelling at the london vaac: A review of developments since the 2010 Eyjafjallajökull volcano ash cloud. *Atmosphere*, *11*(4), 352.

Bonadonna, C., Genco, R., Gouhier, M., Pistolesi, M., Cioni, R., Alfano, F., . . . Ripepe, M. (2011). Tephra sedimentation during the 2010 Eyjafjallajökull eruption (Iceland) from deposit, radar, and satellite observations. *Journal of Geophysical Research: Solid Earth*, *116*(B12).

Bonadonna, C., & Phillips, J. C. (2003). Sedimentation from strong volcanic plumes. *Journal of Geophysical Research: Solid Earth*, *108*(B7).

Casadevall, T. J. (1994). The 1989–1990 eruption of Redoubt volcano, Alaska: impacts on aircraft operations. *Journal of volcanology and geothermal research*, *62*(1-4), 301–316.

Cole, R., White, J., Conway, C., Leonard, G., Townsend, D., & Pure, L. (2018).

The glaciovolcanic evolution of an andesitic edifice, South Crater, Tongariro volcano, New Zealand. *Journal of Volcanology and Geothermal Research*, *352*, 55–77.

Del Bello, E., Taddeucci, J., Scarlato, P., Andronico, D., Scollo, S., Kueppers, U., ... others (2017). Effect of particle volume fraction on the settling velocity of volcanic ash particles: insights from joint experimental and numerical simulations. *Scientific reports*, *7*(1), 1–11.

Dunn, M. G., & Wade, D. (1994). Influence of volcanic ash clouds on gas turbine engines. In *Volcanic ash and aviation safety: Proceedings of the first international symposium on volcanic ash and aviation safety* (Vol. 2047, p. 107e117).

Eichelberger, J. C., Keith, T. E., Miller, T. P., & Nye, C. J. (1995). The 1992 eruptions of Crater Peak vent, Mount Spurr volcano, Alaska: chronology and summary. *US Geol. Surv. Bull*, *2139*, 1–18.

Esposito, R., Badescu, K., Steele-MacInnis, M., Cannatelli, C., De Vivo, B., Lima, A., ... Manning, C. E. (2018). Magmatic evolution of the campi flegrei and procida volcanic fields, italy, based on interpretation of data from well-constrained melt inclusions. *Earth-Science Reviews*, *185*, 325–356.

Field, L., Blundy, J., & Yirgu, G. (2008). The magmatic evolution of Dabbahu volcano, Afar, Ethiopia. In *AGU fall meeting abstracts* (Vol. 2008, pp. V21B–2103).

Fisher, R. V., & Schmincke, H.-U. (1984). Pyroclastic fragments and deposits. In *Pyroclastic rocks* (pp. 89–124). Springer.

Francalanci, L., Varekamp, J., Vougioukalakis, G., Delant, M., Innocenti, F., & Manetti, P. (1995). Crystal retention, fractionation and crustal assimilation in a convecting magma chamber, Nisyros volcano, Greece. *Bulletin of Volcanology*, *56*(8), 601–620.

Gislason, S. R., Hassenkam, T., Nedel, S., Bovet, N., Eiriksdottir, E. S., Alfredsson, H. A., ... others (2011). Characterization of Eyjafjallajökull volcanic ash particles and a protocol for rapid risk assessment. *Proceedings of the National Academy of Sciences*, *108*(18), 7307–7312.

Guffanti, M., & Tupper, A. (2015). Volcanic ash hazards and aviation risk. In *Volcanic hazards, risks and disasters* (pp. 87–108). Elsevier.

Haddadi, B., Sigmarsson, O., & Larsen, G. (2017). Magma storage beneath grímsvötn volcano, iceland, constrained by clinopyroxene-melt thermobarometry and volatiles in melt inclusions and groundmass glass. *Journal of Geophysical Research: Solid Earth*, *122*(9), 6984–6997.

Horwell, C. J. (2007). Grain-size analysis of volcanic ash for the rapid assessment of respiratory health hazard. *Journal of Environmental Monitoring*, *9*(10), 1107–1115.

Horwell, C. J., & Baxter, P. J. (2006). The respiratory health hazards of volcanic ash: a review for volcanic risk mitigation. *Bulletin of volcanology*, *69*, 1–24.

Keiding, J. K., & Sigmarsson, O. (2012). Geothermobarometry of the 2010 Eyjafjallajökull eruption: New constraints on Icelandic magma plumbing systems. *Journal of Geophysical Research: Solid Earth*, *117*(B9).

Kenedi, C. A. (2000). *Volcanic ash fall–a" hard rain" of abrasive particles*. US Department of the Interior, US Geological Survey.

Krishnan, G., Achyuthan, H., & Siva, V. (2017). Comparative petrophysical and geochemical characteristics of thermal and volcanic ash from southeastern India. *Journal of the Geological Society of India*, *90*, 20–24.

Lara, L. E. (2009). The 2008 eruption of the Chaitén volcano, Chile: a preliminary report. *Andean geology*, *36*(1), 125–129.

Larsen, J. F., Nye, C. J., Coombs, M. L., Tilman, M., Izbekov, P., & Cameron, C. (2010). Petrology and geochemistry of the 2006 eruption of Augustine volcano. In J. A. Power, M. L. Coombs, & J. T. Freymueller (Eds.), *The 2006 eruption of Augustine volcano, Alaska* (Vol. 1769, p. 335-382).

Larsen, J. F., Śliwiński, M. G., Nye, C., Cameron, C., & Schaefer, J. R. (2013). The 2008 eruption of Okmok Volcano, Alaska: Petrological and geochemical constraints on the subsurface magma plumbing system. *Journal of Volcanology and Geothermal Research*, *264*, 85–106.

Lau, W. S., Grainger, R. G., & Taylor, I. (2023). *Volcanic ash density.* University of Oxford. doi: 10.5287/ora-r1dqbnpab

Longchamp, C., Bonadonna, C., Bachmann, O., & Skopelitis, A. (2011). Characterization of tephra deposits with limited exposure: the example of the two largest explosive eruptions at Nisyros volcano (Greece). *Bulletin of Volcanology*, *73*(9), 1337–1352.

Miyabuchi, Y., Watanabe, K., & Egawa, Y. (2006). Bomb-rich basaltic pyroclastic flow deposit from Nakadake, Aso volcano, southwestern Japan. *Journal of volcanology and geothermal research*, *155*(1-2), 90–103.

NASA. (1976). *US standard atmosphere, 1976* (Vol. 76) (No. 1562). National Oceanic and Atmospheric Administration.

Nye, C. J., Swanson, S. E., Avery, V. F., & Miller, T. P. (1994). Geochemistry of the 1989–1990 eruption of Redoubt volcano: Part i. whole-rock major-and trace-element chemistry. *Journal of Volcanology and Geothermal Research*, *62*(1-4), 429–452.

Parfitt, L., & Wilson, L. (2009). *Fundamentals of physical volcanology.* John Wiley & Sons.

Pieri, D., Ma, C., Simpson, J., Hufford, G., Grindle, T., & Grove, C. (2002). Analyses of in-situ airborne volcanic ash from the February 2000 eruption of Hekla volcano, Iceland. *Geophysical Research Letters*, *29*(16), 19–1.

Pistolesi, M., Cioni, R., Bonadonna, C., Elissondo, M., Baumann, V., Bertagnini, A., ... Francalanci, L. (2015). Complex dynamics of small-moderate volcanic events: the example of the 2011 rhyolitic Cordón Caulle eruption, Chile. *Bulletin of Volcanology*, *77*(1), 1–24.

Prata, A., Grainger, R., Taylor, I., Povey, A., Proud, S., & Poulsen, C. (2022). Uncertainty-bounded estimates of ash cloud properties using the ORAC algorithm: application to the 2019 Raikoke eruption. *Atmospheric Measurement Techniques*, *15*, 5985–6010.

Prata, G., Ventress, L., Carboni, E., Mather, T., Grainger, R., & Pyle, D. (2019). A new parameterization of volcanic ash complex refractive index based on NBO/T and SiO2 content. *Journal of Geophysical Research: Atmospheres*, *124*(3), 1779–1797.

Reed, B. E. (2016). *Measurements of the complex refractive index of volcanic ash* (Doctoral dissertation, University of Oxford). Retrieved from `https://ora.ox` `.ac.uk/objects/uuid:6df66964-7e17-4ef5-a984-9a863a74e4e6`

Richards, S., & Bouazza, A. (2007). Determination of particle density using water and gas pycnometry. *Géotechnique*, *57*(4), 403–406.

Rincon, P. (2011). Volcanic ash air shutdown the 'right' decision. *BBC News*.

Rose, W. I., & Durant, A. J. (2009). Fine ash content of explosive eruptions. *Journal of Volcanology and Geothermal Research*, *186*(1-2), 32–39.

Rossi, E., Bagheri, G., Beckett, F., & Bonadonna, C. (2021). The fate of volcanic ash: premature or delayed sedimentation? *Nature communications*, *12*(1), 1–9.

Rousseau, R. M. (2001). Detection limit and estimate of uncertainty of analytical XRF results. *Rigaku J*, *18*(2), 33–47.

Rust, A., & Cashman, K. (2011). Permeability controls on expansion and size distributions of pyroclasts. *Journal of Geophysical Research: Solid Earth*, *116*(B11).

Scasso, R. A., Corbella, H., & Tiberi, P. (1994). Sedimentological analysis of the tephra from the 12–15 August 1991 eruption of Hudson volcano. *Bulletin of Volcanology*, *56*(2), 121–132.

Smirnov, S., Nizametdinov, I., Timina, T., Kotov, A., Sekisova, V., Kuzmin, D., ... Abersteiner, A. (2021). High explosivity of the June 21, 2019 eruption of Raikoke volcano (Central Kuril Islands); mineralogical and petrological constraints on the pyroclastic materials. *Journal of Volcanology and Geothermal Research*, *418*, 107346.

Sparks, R. S. J., Bursik, M., Carey, S., Gilbert, J., Glaze, L., Sigurdsson, H., & Woods, A. (1997). *Volcanic plumes.* Wiley.

Sparks, R. S. J., & Wilson, L. (1976). A model for the formation of ignimbrite by gravitational column collapse. *Journal of the Geological Society*, *132*(4), 441–451.

Sparks, R. S. J., Wilson, L., & Sigurdsson, H. (1981). The pyroclastic deposits of the 1875 eruption of Askja, Iceland. *Philosophical Transactions of the Royal Society of London. Series A, Mathematical and Physical Sciences*, *299*(1447), 241–273.

Vogel, A., Diplas, S., Durant, A., Azar, A. S., Sunding, M. F., Rose, W. I., ... Stohl, A. (2017). Reference data set of volcanic ash physicochemical and optical properties. *Journal of Geophysical Research: Atmospheres*, *122*(17), 9485–9514.

Walker, G. P. (1993). Basaltic-volcano systems. *Geological Society, London, Special Publications*, *76*(1), 3–38.

Webb, P. A., & Orr, C. (1997). *Analytical methods in fine particle technology.* Micromeritics Instrument Corporation.

Wehrmann, H., Bonadonna, C., Freundt, A., Houghton, B. F., & Kutterolf, S. (2006). Fontana tephra: a basaltic Plinian eruption in Nicaragua. *Special Papers - Geological Society of America*, *412*, 209.

White, F. M., & Majdalani, J. (2006). *Viscous fluid flow* (Vol. 3). McGraw-Hill New York.

Wilson, L., & Huang, T. C. (1979). The influence of shape on the atmospheric settling velocity of volcanic ash particles. *Earth and Planetary Science Letters*, *44*(2), 311–324.

Wilson, M. (1989). *Igneous petrogenesis.* Springer.